Nanoscale

PAPER

Cite this: *Nanoscale*, 2017, **9**, 1653

How the alignment of adsorbed *ortho* H pairs determines the onset of selective carbon nanotube etching†

U. Khalilov,*[a] A. Bogaerts,[a] B. Xu,[b] T. Kato,[b] T. Kaneko[b] and E. C. Neyts[a]

Received 12th October 2016,
Accepted 15th December 2016

DOI: 10.1039/c6nr08005g

www.rsc.org/nanoscale

Unlocking the enormous technological potential of carbon nanotubes strongly depends on our ability to specifically produce metallic or semiconducting tubes. While selective etching of both has already been demonstrated, the underlying reasons, however, remain elusive as yet. We here present computational and experimental evidence on the operative mechanisms at the atomic scale. We demonstrate that during the adsorption of H atoms and their coalescence, the adsorbed *ortho* hydrogen pairs on single-walled carbon nanotubes induce higher shear stresses than axial stresses, leading to the elongation of HC–CH bonds as a function of their alignment with the tube chirality vector, which we denote as the γ-angle. As a result, the C–C cleavage occurs more rapidly in nanotubes containing *ortho* H-pairs with a small γ-angle. This phenomenon can explain the selective etching of small-diameter semiconductor nanotubes with a similar curvature. Both theoretical and experimental results strongly indicate the important role of the γ-angle in the selective etching mechanisms of carbon nanotubes, in addition to the nanotube curvature and metallicity effects and lead us to clearly understand the onset of selective synthesis/removal of CNT-based materials.

Introduction

A major difficulty for applying single-wall carbon nanotubes (SWNTs) to nano-electronics is that almost all the current available synthesis techniques produce a mixture of semiconducting (s-SWNTs) and metallic SWNTs (m-SWNTs).[1,2] Therefore, the fabrication of SWNT materials containing either a high fraction of s-SWNTs[3–14] or m-SWNTs[15–17] is highly important.

In addition to selective growth[4] and post-synthesis separation techniques,[2] nanotubes with the desired properties may also be prepared *in situ*. Zhang and co-workers[3] presented selective etching of metallic nanotubes by hydrocarbonation, retaining the semiconducting nanotubes in a near-pristine form. They reported that permanent removal of m-SWNTs from the wafers is achieved with H-atoms in addition to H^+ and CH_3^+ ions in methane plasma. Also, Hassanien *et al.*[12] and Kato *et al.*[18] reported selective etching of m-SWNTs or a concentration increase of s-SWNTs using hydrogen plasma. Huang *et al.*[10] demonstrated preferential etching of m-SWNTs over s-SWNTs through laser irradiation in air. The effect was ascribed to the different rates of the photolysis-assisted oxidation of the tubes. Zhang *et al.*[7] reported the fabrication of well-aligned individual s-SWNTs by Xe-lamp irradiation. Specifically, m-SWNTs, irrespective of their diameters, and s-SWNTs with diameters less than 1 nm were preferentially destroyed. The preferential etching of the m-SWNTs over the s-SWNTs was demonstrated by *in situ I–V* measurements, showing a 200-fold increase in on/off ratios for FETs fabricated from the as-grown SWNT arrays. Also, Shim *et al.*[11] reported preferential destruction of m-SWNTs using microwave irradiation. In this case, well-aligned s-SWNTs were prepared by using water vapor as a weak oxidant to etch the m-SWNTs during or after SWNT growth.[8]

On the other hand, Hou *et al.*[17] reported a sample enriched with m-SWNTs. They initially obtained small diameter s-SWNTs and large diameter m-SWNTs by tuning the experimental parameters. Subsequently, due to curvature and temperature effects,[3] small-diameter s-SWNTs were preferentially removed by adding hydrogen as an etchant gas at a higher temperature. However, they do not comment on either small-diameter m-SWNTs or large-diameter s-SWNTs. Harutyunyan and co-workers[16] also reported preferential growth of

[a]*Department of Chemistry, Research Group PLASMANT, University of Antwerp, Universiteitsplein 1, 2610 Wilrijk, Antwerp, Belgium.*
E-mail: umedjon.khalilov@uantwerpen.be; Fax: +32-3-265 23 43;
Tel: +32-3-265 23 82
[b]*Department of Electronic Engineering, Tohoku University, 6-6-05 Aoba, Aramaki, Aoba-ku, Sendai 980-8579, Japan*
†Electronic supplementary information (ESI) available. See DOI: 10.1039/c6nr08005g

m-SWNTs by varying the noble gas atmosphere during thermal annealing of the catalyst, and in combination with oxidative and reductive species, they noted, however, that the presence of H_2 alone in the atmosphere does not lead to the preferential growth of metallic tubes.

All aforementioned results indicate that metallic nanotubes are preferentially etched over semiconducting tubes with a similar diameter. However, the underlying reasons remain elusive as yet. Particularly, the etching onset and thus the overall H etching mechanism is still unclear. The atomic structure of a CNT can undergo severe physical distortions and even structural changes, *e.g.*, when H-atoms interact with its cylindrical graphene wall(s). For example, molecular dynamics demonstrated that upon hydrogenation, CNTs deform and expand with increasing H-coverage.[19] The local nanotube curvature adds a fractional sp^3 character to the dominant sp^2 bonding character, especially in narrow SWNTs, making them more reactive and prone to hydrogen chemisorption.[3,20] Chemisorbed hydrogen, in turn, significantly modifies the structure and stability of the nanotubes and increases the inter-tube distance. Furthermore, experimental results indicate that such irreversible structural changes to the CNT structure can begin when the H dose,[18,21,22] H-atom exposure temperature[21,23] and plasma power or H-exposure time[19,22,24] are increased. Moreover, the incident H-atoms, which are generated in the H_2 plasma, amorphize and subsequently etch the cylindrical graphene walls of the nanotube.[25] Once an etch pit is formed, etching proceeds rapidly, and the remainder of the CNT is quickly etched away.[22,25] The reactions with H-atoms occur much faster for cylindrical graphite rather than for planar graphite, suggesting that the curvature enhances the reactivity.[24–27]

Despite the aforementioned investigations, however, the etching onset and thus the precise mechanism of hydrogen-based CNT etching is still not clearly understood. We here provide evidence that nanotube etching is fundamentally caused by H-adsorption induced stress depending on the alignment of adsorbed H-pairs, in addition to the nanotube curvature and metallicity effects.

Methods

MD/tfMC and ReaxFF

Hybrid classical molecular dynamics/time-stamped force-bias Monte Carlo (MD/tfMC) simulations were used to follow the system evolution during H-bombardment and H-etching. The tfMC technique can very efficiently be coupled to canonical MD simulations.[28–30] Using this hybrid method, the initial chemical reactions take place during the first few picoseconds in the MD module and subsequently the longer time scale relaxation of the system is taken care of in the MC module. During both MD and MC calculations, all atomic interactions, including bond associations and dissociations, are described by the ReaxFF,[31] using parameters developed by Mueller *et al.*[32] Note that the time and length scales of the problem at hand prohibit the use of computationally expensive DFT calculations or more accurate alternative approaches. Application of the combined tfMC/MD technique was previously demonstrated to allow the description of relaxation processes in general, and the simulation of the CNT nucleation process in particular, in a much more efficient way compared to pure MD simulations.[33–35]

MD/tfMC simulation details

Etch mechanisms are evaluated on armchair (5,5) and (8,8) tubes, on zigzag (8,0) and (14,0) tubes, as well as on chiral (6,4) and (7,2) CNTs. The calculated radii of the selected nanotubes are in close agreement with the experimental values. Periodic boundary conditions are applied along the *z*-axis, corresponding to a unit cell length longer than 2 nm, to mimic an infinitely long nanotube. Prior to subjecting the tubes to etching, they are thermalized and relaxed. All structures were equilibrated at the desired temperature using NpT (Berendsen thermo/barostat[36]) and subsequently canonical NVT (Bussi thermostat[37]) ensembles. The calculated radial, tangential and axial stresses of the relaxed nanotubes prior to hydrogenation are shown in Fig. S1 in the ESI.† The total number of H atoms is kept constant throughout all simulations. When a H atom adsorbs on the tube, the resulting structure is allowed to relax by application of tfMC. During this relaxation stage, no new atoms are allowed to impinge on the CNT.

DFT calculations

All density functional theory (DFT) calculations were carried out using pseudoatomic orbitals (PAOs) implemented in the OpenMX code.[38] The exchange–correlation energy in the generalized gradient approximation is described by the Perdew–Burke–Ernzerhof functional (GGA-PBE).[39] The electron–ion interaction was treated using norm-conserving pseudopotentials[40] with partial core corrections.[41] A plane wave cut-off energy of 150 Ry was applied. The convergence criterion of the forces on the atoms for all geometry optimizations was set to 0.005 eV $Å^{-1}$.

Hydrogen plasma irradiation

Plasma irradiation was carried out by using a laboratory-made diffusion plasma system. The SWNTs coated on a SiO_2 substrate were placed in the diffusion region of the plasma (45 mm away from the bottom electrode) during plasma irradiation. Further detailed experimental information is shown in the ESI (see Fig. S2†).

Chirality selective etching of s-SWNTs

High-pressure CO conversion (HiPco) SWNTs were used as a starting material for this experiment. The chirality distributions of SWNTs were analyzed by UV-Vis-NIR spectroscopy. After plasma irradiation, the SWNTs were dispersed into a sodium chloride solution (~2 wt%) by 2 h ultrasonication followed by 2 h centrifugation (30 000*g*) to obtain individually-dispersed SWNT suspensions.

Preferential etching of m-SWNTs

Chemically purified metallic and semiconductor SWNTs (NanoIntegris) were used as a starting material. The etching rate of metallic and semiconducting SWNTs was estimated from the time evolution data of Raman scattering spectroscopy measured with He–Ne laser (wavelength: 632.8 nm) excitation. Variation of Raman scattering spectra as a function of plasma irradiation time was taken from the same SWNT sample by repeating 10 s plasma irradiation followed by spatial Raman mapping measurements.

Results and discussion

CNT curvature change

Due to pyramidalization and misalignment of the π-orbitals of the C atoms,[26] the adsorption barrier decreases and the nanotube reactivity increases significantly compared to a flat graphene sheet.[25,42] In the hydrogenation process, therefore, the impinging H atom or H_2 molecule can physically adsorb easily and consequently (dissociatively) chemisorb on the small-diameter CNTs.[42–44] Moreover, adsorbed hydrogen atoms diffuse over the nanotube wall and form local surface clusters.[45–47]

In Fig. 1, the H clustering effect on the nanotube local curvature is shown. When a single H-atom adsorbs onto a C atom, the sp^2 character of both the C atom and its neighbors converts to quasi sp^3, which leads to an increase in the local curvature of the nanotube and an increase in the reactivity of these sites. Therefore, an incoming H atom or H_2 molecule adsorbs nearby or moves towards the first chemisorbed H, thus creating either *para* (red–red or blue–red H atoms), *ortho* (blue–blue H atoms) or *meta* (blue–green or red–green H atoms) pairs,[43,45,47–49] as shown in Fig. 1, side view. Due to the weak adsorption behavior of unstable *meta* pairs, *para* and *ortho* configurations (with negative interaction energies in the range of 0.11–0.44 eV) are preferred, which is in agreement with hydrogen pairs on both planar[47,48] and curved[20,43,45,49,50] graphitic surfaces. The interaction energy of the H atom with the CNT is defined as $E_{int} = E_{CNT-H} - (E_{CNT} + \frac{1}{2}E_{H_2})$, where E_{CNT-H}, E_{CNT} and E_{H_2} are the total energies of the fully optimized CNT–H structure, single nanotube and H_2 molecule, respectively. Due to the appearance of quasi sp^3 neighbor C atoms, H atoms can adsorb or move towards this reduced barrier site (see Fig. S3 and S4 in the ESI†) and the hydrogen concentration thus significantly increases in this region. Such an ordering and clustering effect has also been observed in DFT-based calculations on both graphene and SWNTs partially covered with hydrogen.[20,45,47] Also, new incoming H atoms can adsorb or move to opposite ends of the (now elliptical) structure due to the increased local curvature (see Fig. S4 in the ESI†). Adsorbed hydrogen atoms thus have the tendency to cluster on both sides of the elliptical nanotube and hydrogenation can eventually lead to formation of parallel nanotube ribbons.[51] Generally, our results show that clustering of H atoms can significantly increase the local curvature, which eventually leads to initiate CNT etching during the hydrogenation process.

Note also that hydrogen atoms adsorb and cluster, but may also desorb either by the Langmuir–Hinshelwood recombinative desorption or the Eley–Rideal abstraction mechanisms during hydrogenation.[52–54] Due to hydrogen desorption as well as its low sticking probability, the nanotube surface is not fully covered by a hydrogen "shell". At low temperature, the coverage reaches about 20% before stagnating (see Fig. S5 in the ESI†) in agreement with experimental evidence: a similar adsorption trend at room temperature was reported with a total residual H_2 storage capacity between 21 and 25%.[55] At high temperature (1600 K), however, the coverage rises steeply and does not stagnate due to the easy breaking of C–C bonds in the nanotube; at about 15% and 27% coverage, the armchair and zigzag nanotubes are getting etched, respectively.

During the hydrogenation, the formation of all three H-pairs is random and their number is low due to simultaneous H_2 desorption. In the hydrogen clustering, both *para* and *ortho* configurations are found on the tube surface, whereas *meta*-pairs are much less frequently observed. It is invariably the *ortho* pairs, however, which are responsible for the initial C–C bond breaking, determining the onset of the CNT etching.

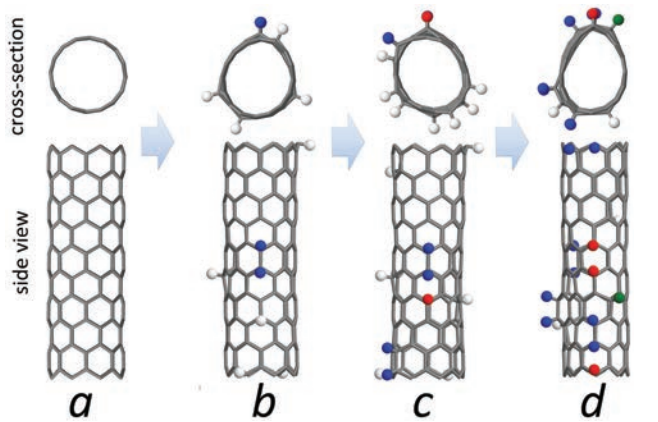

Fig. 1 Change in nanotube curvature during the hydrogenation after coalescence of H adatoms, forming *para* (red–red or blue–red H pairs), *ortho* (blue–blue H pairs) and *meta* (blue–green or red–green H pairs) configurations on the tube. For the sake of clarity, C atoms of the tube are not shown. During the hydrogenation, H coverage consecutively changes from 0 (a) to 4% (b), 8% (c) and 9% (d).

γ-Angle

To understand the reason for the initial C–C bond breaking, hydrogen interaction with armchair, zigzag and chiral nanotubes with a similar curvature (*i.e.*, diameters in the range of 0.64–0.7 nm) and with different possible *ortho* H-pairs are investigated, as shown in Fig. 2. In order to distinguish different aligned *ortho* pairs, we introduce γ, the characteristic angle between an *ortho* HC–CH bond and the C_h chirality vector. The arrangement of *ortho* bonds on the same tube is easily differentiated by three γ-angles, *i.e.*, $\gamma_1 = 30° - \theta$, $\gamma_2 = 30° + \theta$ and $\gamma_3 = 90° - \theta$, respectively (where θ is the chiral

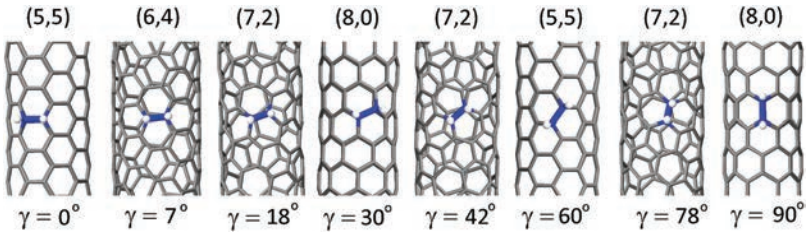

Fig. 2 Possible *ortho* HC–CH bonds (in blue) on the armchair, zigzag and chiral nanotubes. γ is the angle between an *ortho* HC–CH bond and the chirality vector of the nanotube.

Table 1 Dependence of HC–CH lengths on the global shear and axial strains, as obtained from the MD calculations

			γ = 0°	γ = 30°	γ = 60°	γ = 90°
$(d_{HC-CH}/d_{C-C}) - 1$, %	Shear	13%	No bond	16.1	14.1	13
		19%	No bond	No bond	14	13
	Axial	4%	16.3	17	17.2	16.3

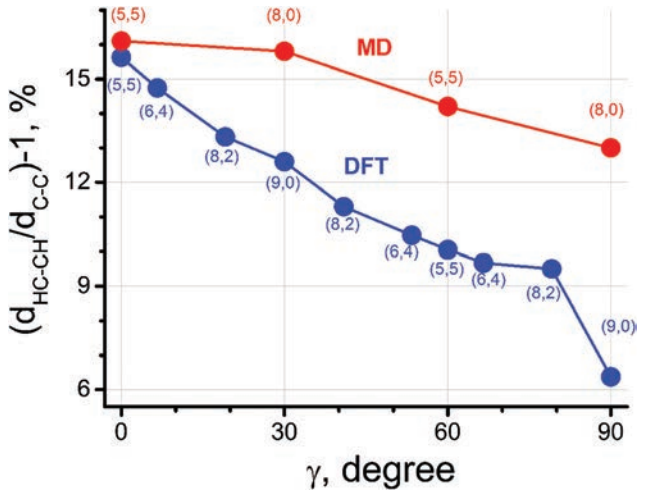

Fig. 3 Dependence of the elongation of the C–C bond with *ortho* H-pairs on the γ-angle. The chirality of the different carbon nanotubes are given in parenthesis. The results obtained by MD and DFT are colored red and blue, respectively.

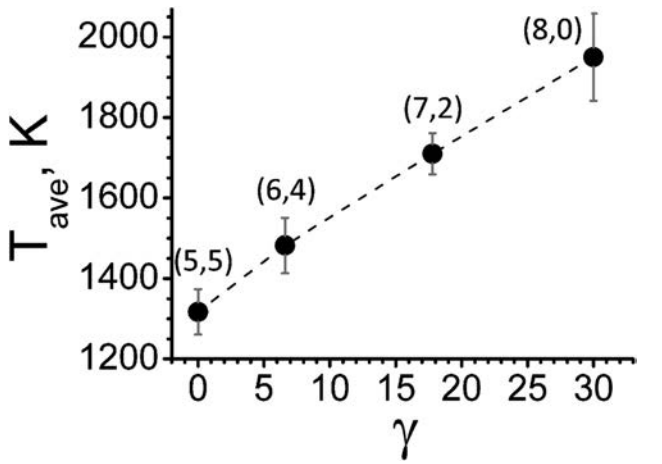

Fig. 4 Temperature for breaking of aligned *ortho* HC–CH bonds on single-walled nanotubes with γ = 0°, 7°, 18° and 30° for (5,5), (6,4), (7,2) and (8,0) tubes, respectively.

angle of the CNT). For example, on the chiral (7,2) nanotube, three different *ortho* bonds with angles of about 18°, 42° and 78°, respectively, are found. In zigzag and armchair nanotubes, however, two of the γ-angles are identical. Therefore, the *ortho* pairs on the (8,0) zigzag tube can be positioned either perpendicular to the chiral vector, *i.e.*, 90°, or they form an angle of 30°. Similarly, on the (5,5) armchair tube, they are either parallel to the vector (*i.e.*, 0°), or they form an angle of 60°.

While a single *ortho* HC–CH bond hardly affects the tube curvature, it can significantly affect the C–C bond length. We found that the length of *ortho* HC–CH bonds increases with decreasing γ-angle. Due to the H adsorption, the HC–CH bond elongates from 13% to 16% in our MD calculations and from 6.5% to 15.5% in our DFT calculations, respectively, both depending inversely on γ, which varies between 0° and 90°. While these results differ quantitatively depending on the calculation technique, the γ-dependence of the HC–CH bond elongation is qualitatively the same. Also, we found that the H–H bond length (2.11 Å–2.25 Å) and CCH-angle (102°–110°) in the *ortho* HC–CH bond are proportional to the γ-angle, which may affect the H adsorption energy.

The results show that C–C cleavage occurs easily due to higher strains in the *ortho* HC–CH bonds with minimum γ-angles. In Table 1, we show the calculated HC–CH *ortho* bond length elongation due to applied shear and axial strains as a function of γ, for γ corresponding to 0°, 60° and 30°, 90° for (5,5) and (8,0) nanotubes, respectively. In the case of γ = 0° and γ = 30°, the maximum C–C bond length is deformed by 16.3% and 17%, respectively, when an axial tensile strain of

4% is applied. When a shear strain of 13% is applied, the C–C bond is broken for $\gamma = 0°$, while a shear strain of 19% yields a broken C–C bond in the case of $\gamma = 0°$ or 30°. It is therefore likely that in those configurations, the C–C bond can easily break due to thermal fluctuations. In the configurations corresponding to $\gamma = 60°$ and $\gamma = 90°$, the maximum C–C bond length deformation is observed when an axial tensile strain of 4% is applied. In that case, the C–C bond length is elongated by 17.2% and 16.3%, respectively. When a shear strain between 13% and 19% is applied, or when no strain is applied at all, the C–C bond length increases by 14% and 13% for $\gamma = 60°$ and $\gamma = 90°$, respectively. Note that in the case of $\gamma = 90°$, applying a shear strain has no influence at all on the bond length. The results indicate that the elasticity is closer to tube failure in the radial direction than in the axial direction. The key point is that in all cases, hydrogen adsorption leads to a significant C–C bond length increase due to the adsorption-induced shear strain. Such a mechanical–chemical effect in the process of hydrogenation of highly twisted carbon nanotubes was also investigated using reactive MD simulations.[56] It is well known that such deformed and strained structures naturally appear due to CNT breathing with increasing temperature.[19,57]

The influence of temperature on the breaking of aligned *ortho* HC–CH bonds is shown in Fig. 4. The graph illustrates that the average temperature for C–C breaking is 1317 K, 1482 K, 1710 K and 1950 K for the *ortho* configurations on (5,5), (6,4), (7,2) and (8,0) tubes with minimum γ-angles of 0°, 7°, 18° and 30°, respectively. The *ortho* HC–CH bonds, already elongated due to adsorption of *ortho* H pairs, can be broken when the temperature increases: the temperature increase induces more (initially non-zero) shear stresses rather than (initially zero) axial stresses[58] on the nanotube (see Fig. S1 in the ESI†). As a result, the trend plotted in Fig. 4 indicates that *ortho* bonds with a smaller γ-angle are more easily broken due to thermal fluctuations (or CNT radial breathing[57]), which eventually leads to etching of the nanotube.

Due to the high concentration of adsorbed hydrogen, small diameter SWNTs can also be etched or cut at low temperature (see Fig. S6 in the ESI†). Our simulations demonstrate that the etching process at 300 K is initiated by this strained *ortho* C–C breaking due to an increase of the local curvature of the (5,5) nanotube during the coalescence of adsorbed hydrogen atoms. After breaking of this C–C bond, the average distance between the C atoms involved is 2.9 Å. The distance between their respective H atoms is 2.1 Å: these values agree well with zero Kelvin *ab initio* calculation results of 2.77 Å and 2.18 Å, respectively.[20] Such C–C bond breaking eventually leads to etching or cutting the small-diameter nanotube at low temperature, which is in agreement with experimental evidence.[22]

To clarify the role of the γ-angle in CNT etching with H_2 plasma, we provide experimental evidence in Fig. 5. Due to the high reactivity and thus high adsorption probability of H atoms, metallic ($E_g = 0$) or semi-metallic ($E_g \approx 0$) CNTs are very quickly etched. To avoid the metallicity and curvature effects, we select semiconductor ($E_g \approx 1$ eV) CNTs, *i.e.*, (6,5), (7,5) and (8,3) with diameters of 0.747 nm, 0.818 nm and 0.772 nm, respectively. The minimum γ is equal to 3°, 5.5° and 14.7°, respectively, for these tubes. Since the absorbance ($I_{ab}(t)$) of (n,m) chirality CNTs is proportional to the area of the graphitic structure in (n,m) chirality SWNTs, we estimated the etching probability of each (n,m) chirality CNT from the vari-

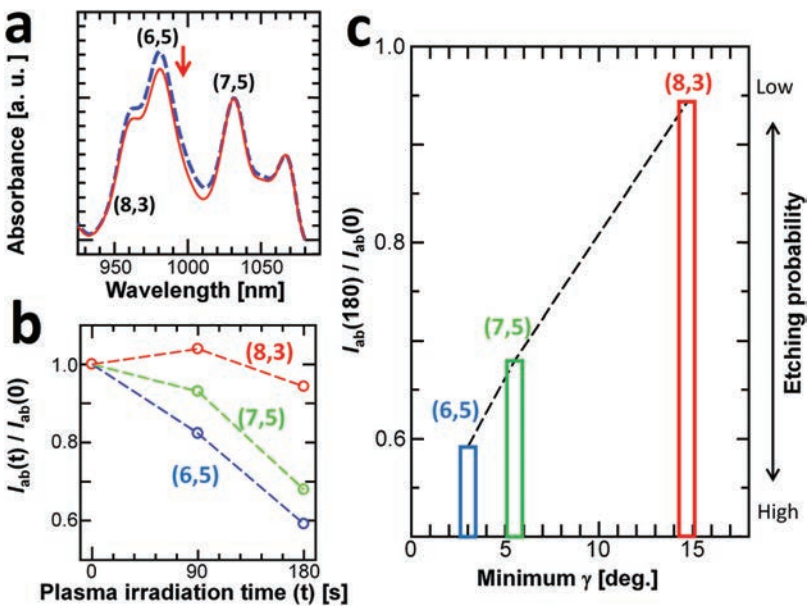

Fig. 5 (a) Typical raw UV-vis-NIR absorption spectra of HiPco CNTs before (dashed blue curve) and after 180 s (solid red curve) H_2 plasma irradiation. The absorbance was normalized by that of the (7,5) CNT for each spectrum. The red arrow indicates the preferential depletion of the (6,5) component after plasma irradiation. (b) Normalized UV-vis-NIR absorption ($I_{ab}(t)/I_{ab}(0)$) for each chirality as a function of plasma irradiation time (t). (c) Histogram of $I_{ab}(180)/I_{ab}(0)$ plotted with minimum γ.

ation of $I_{ab}(t)$ as a function of H_2 plasma irradiation time (t). The $I_{ab}(t)$ for each (n,m) chirality CNT was measured by decomposing UV-vis-NIR spectra with multiple Lorentzian curve fitting (Fig. 5(a)). Since $I_{ab}(t)$ is sensitive to the chiralities, $I_{ab}(t)$ was normalized by the data before plasma irradiation (t = 0 s) for each (n,m) chirality CNT, enabling to discuss the chirality dependence of the etching probability. Interestingly, the time evolution of $I_{ab}(t)/I_{ab}(0)$ clearly varies for each chirality species. This indicates that there is a chirality dependence for the etching probability of CNTs (Fig. 5(b)). Then, $I_{ab}(t)/I_{ab}(0)$ at t = 180 s is replotted as a function of minimum γ (Fig. 5(c)). The $I_{ab}(180)/I_{ab}(0)$ ratio of (6,5) CNTs shows a minimum value and increases with minimum γ, denoting that the etching probability of each chirality CNT decreases with an increase in minimum γ. This is consistent with the results of the calculations shown in Fig. 4.

The overall results indicate that the effect of the γ-angle should also be taken into account in the CNT hydrogenation and its etching, in addition to the curvature,[24,26] temperature[22,51] and metallicity[56–61] effects. The *ortho* H pairs more perpendicular to the tube axis ($\gamma \rightarrow 0°$) are responsible for the C–C bond breaking for single-walled nanotubes. The distortion of the *ortho* C–C bonds depends on the local curvature, and increases due to both the clustering of adsorbed H atoms and the temperature-dependent nanotube breathing. It is thus the combination of CNT breathing, C–C bond elongation upon strain when H-covered, and thermal fluctuations which eventually leads to initiation of the etching of carbon nanotubes.

H etching mechanism of CNTs

Based on these findings and previous experimental[1,22,24,25] and theoretical/computational[19,20,26,45,61] studies, we can now unravel the H etching scenario for carbon nanotubes. As depicted in Fig. 6, three stages can be distinguished: (1) H adsorption and clustering, subsequent (2) defect creation and finally (3) etch initiation (or etch pit formation).

In the first stage, H atoms or H_2 molecules (dissociatively) adsorb on the surface and cluster, leading to the occupation of neighboring sites as described above (Fig. 6a). Regarding previous experimental and theoretical results, both the nanotube curvature (and thus diameter)[22,24,26] and its electronic structure[59–61] play an important role in increasing the chemical reactivity of small-diameter nanotubes in this stage. In large diameter nanotubes, however, the nanotube reactivity merely depends on its metallicity due to its lower curvature. Incoming H atoms or H_2 molecules preferentially adsorb on metallic single-walled nanotubes rather than on semi-metallic and semiconducting tubes due to its zero band gap, followed by clustering. Such clustering of H atoms[45] can increase the local curvature of the nanotube (see Fig. 1) and subsequently weaken the C–C bonds at that site.

The second stage starts when the first defect appears due to breaking of an *ortho* C–C bond with a minimum γ-angle (*i.e.*, HC–CH bond alignment to the chirality vector) (Fig. 6b). We found that the minimum γ-angle is responsible for the bond breaking after the local change in the nanotube curvature. Also, the effect of temperature-dependent nanotube breathing enhances the C–C breaking at high temperatures. The most significant C–C bond breaking is found for armchair tubes due to their *ortho* HC–CH bonds with γ = 0°, which are thus more likely to be etched compared to zigzag tubes (see Fig. S7 in the ESI†). The C–C bond breaking in both nanotubes is due to the presence of strained HC–CH *ortho* bonds with γ = 0° and γ = 30°, respectively. However, the γ = 0° *ortho* bonds are more prone to breaking (*cf.* Table 1 and Fig. 3 and 4), which indicates why armchair (metallic) nanotubes are indeed preferentially etched over zigzag (semiconducting or semi-metallic) nanotubes (see Fig. S8 in the ESI†). Furthermore, the effect of the γ-angle explains the selective etching of semiconducting nanotubes with a similar diameter *via* H_2-plasma (Fig. 5). Moreover, we can suggest that H adsorption increases due to both the metallicity[61] and the γ-angle, and thus semi-metallic (chiral or zigzag) tubes are also etched faster than semiconducting tubes.

In the third stage, additional *ortho* pairs of H-atoms rapidly occupy nearby neighboring sites, leading to the formation of a hole or so-called etch pit, as shown in Fig. 6c (see also the last frame of Fig. S6 in the ESI†). The C–C bonds connecting these sites are consecutively broken. This result closely resembles the experimental evidence on graphite and MWNT etching,[25] showing the formation of holes and etch pits upon H-atom exposure. Also in agreement with experiments, we observe in the simulations that the initial etch pit formation occurs at a site on the CNT wall that contains a defect.[25] Moreover, as can be seen in Fig. 6c, the resulting hole in our simulations is surrounded by H-atoms, as was previously also demonstrated experimentally by EELS measurements.[25] This indicates that the carbon atoms in that region remain purely sp^3-bonded. This leads to initiate the fast etching of the CNT, in agreement with the experimental observations.[3,22,25]

In general, the initial C–C bond cleavage (stage 2) is slower than both the hydrogenation/dehydrogenation (stage 1) and etch-pit formation steps (stage 3). NEB-calculations[62] indicate that the energy barrier for C–C bond breaking (0.8 eV) is higher than the H adsorption (0.24 eV) and surface diffusion barriers (0.57 eV). This indicates that the second stage (*i.e.*, the etching onset) is the rate-limiting step in the hydrogenation/etching of carbon nanotubes.

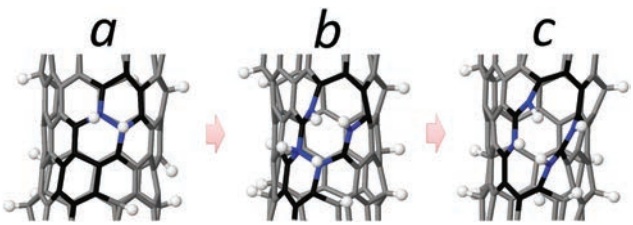

Fig. 6 Defect creation and destruction mechanism of a nanotube: (a) partial hydrogenation of a carbon nanotube; (b) C–C bond breaking in the H-terminated carbon site; (c) creation of a hole (or etch pit) in that site.

Conclusion

Based on our theoretical and experimental results, we unravel the H etching mechanism for carbon nanotubes, which can be subdivided into three consecutive steps: H adsorption and clustering, defect creation and etch pit formation or etch initiation. After adsorption and clustering of H atoms, the local curvature of the tube changes (increases). Such curvature increase leads to elongation of C–C bonds in this area and subsequent breaking of strained *ortho* C–C bonds with a minimum γ-angle, *i.e.*, angle between the *ortho* HC–CH bond and the chirality vector. We found that *ortho* H pairs more perpendicular to the tube axis ($\gamma \rightarrow 0°$) are responsible for C–C bond breaking for single-walled nanotubes, which in turn determines the onset of the CNT etching. Finally, an etch pit is formed due to H occupation of C atoms close to the defect site, inducing further CNT etching. Overall, our results demonstrate that the γ-angle can explain (1) the preferential etching of armchair tubes over zigzag tubes and (2) the selective etching of semiconductor tubes with a similar diameter. Our atomic-scale study strongly indicates that the chirality dependent γ-angle, in addition to the nanotube curvature and its electronic structure, is the key parameter in the selective etching of carbon nanotubes.

Conflict of interest

The authors declare no competing financial interest.

Acknowledgements

U. K. gratefully acknowledges financial support from the Fund of Scientific Research Flanders (FWO), Belgium (Grant No. 12M1315N). This work was also supported in part by Grant-in-Aid for Young Scientists A (Grant No. 25706028), Grant-in-Aid for Scientific Research on Innovative Areas (Grant No. 26107502) from JSPS KAKENHI. This work was carried out in part using the Turing HPC infrastructure at the CalcUA core facility of the Universiteit Antwerpen (UA), a division of the Flemish Supercomputer Center VSC, funded by the Hercules Foundation, the Flemish Government (department EWI) and the UA. The authors also thank Prof. A. C. T. van Duin for sharing the ReaxFF code and J. Razzokov for his assistance to perform the DFT calculations.

References

1 Y. Chen, A. K. Ng, S. Bai, R. Si, L. Wei and Q. Wang, *Separation of Metallic and Semiconducting Single-Wall Carbon Nanotubes*, Pan Stanford Publishing Pte Ltd, 2012, ch. 4.

2 N. Komatsu and F. Wang, A Comprehensive Review on Separation Methods and Techniques for Single-Walled Carbon Nanotubes, *Materials*, 2010, **3**, 3818–3844.

3 G. Zhang, P. Qi, X. Wang, Y. Lu, X. Li, R. Tu, S. Bangsaruntip, D. Mann, L. Zhang and H. Dai, Selective Etching of Metallic Carbon Nanotubes by Gas-Phase Reaction, *Science*, 2006, **304**, 974.

4 L. Qu, F. Du and L. Dai, Preferential Syntheses of Semiconducting Vertically Aligned Single-Walled Carbon Nanotubes for Direct Use in FETs, *Nano Lett.*, 2008, **8**, 2682.

5 L. Ding, *et al.*, Selective growth of well-aligned semiconducting single-walled carbon nanotubes, *Nano Lett.*, 2009, **9**, 800–805.

6 J. Lu, L. Lai, G. Luo, J. Zhou, R. Qin, D. Wang, L. Wang, W. N. Mei, G. Li, Z. Gao, S. Nagase, Y. Maeda, T. Akasaka and D. Yu, Why Semiconducting Single-Walled Carbon Nanotubes are Separated from their Metallic counterparts, *Small*, 2007, **3**, 1566–1576.

7 Y. Zhang, Y. Zhang, X. Xian, J. Zhang and Z. Liu, Sorting out Semiconducting Single-Walled Carbon Nanotube Arrays by Preferential Destruction of Metallic Tubes Using Xenon-Lamp Irradiation, *J. Phys. Chem. C*, 2008, **112**, 3849–3856.

8 P. Li and J. Zhang, Sorting out semiconducting single-walled carbon nanotube arrays by preferential destruction of metallic tubes using water, *J. Mater. Chem.*, 2011, **21**, 11815.

9 Y. Li, S. Peng, D. Mann, J. Cao, R. Tu, K. J. Cho and H. Dai, On the Origin of Preferential Growth of Semiconducting Single-Walled Carbon Nanotubes, *J. Phys. Chem. B*, 2005, **109**, 6968.

10 H. Huang, R. Maruyama, K. Noda, H. Kajiura and K. Kadono, Preferential Destruction of Metallic Single-Walled Carbon Nanotubes by Laser Irradiation, *J. Phys. Chem. B*, 2006, **110**, 7316–7320.

11 H. C. Shim, J.-W. Song, Y. K. Kwak, S. Kim and C.-S. Han, Preferential elimination of metallic single-walled carbon nanotubes using microwave irradiation, *Nanotechnology*, 2009, **20**, 065707.

12 A. Hassanien, M. Tokumoto, P. Umek, D. Vrbanič, M. Mozetič, D. Mihailovič, P. Venturini and S. Pejovnik, Selective etching of metallic single-wall carbon nanotubes with hydrogen plasma, *Nanotechnology*, 2005, **16**, 278–281.

13 B. Yu, C. Liu, P.-X. Hou, Y. Tian, S. Li, B. Liu, F. Li, E. I. Kauppinen and H.-M. Cheng, Bulk Synthesis of Large Diameter Semiconducting Single-Walled Carbon Nanotubes by Oxygen-Assisted Floating Catalyst Chemical Vapor Deposition, *J. Am. Chem. Soc.*, 2011, **133**, 5232–5235.

14 W. Zhou, S. Zhan, L. Ding and J. Liu, General Rules for Selective Growth of Enriched Semiconducting Single Walled Nanotubes with Water Vapor as *in situ* Etchant, *J. Am. Chem. Soc.*, 2012, **134**, 14019–14026.

15 R. Krupke, F. Hennrich, H. von Lohneysen and M. M. Kappes, Separation of metallic from semiconducting single-walled carbon nanotubes, *Science*, 2003, **301**, 344–347.

16 A. R. Harutyunyan, G. Chen, T. M. Paronyan, E. M. Pigos, O. A. Kuznetsov, K. Hewaparakrama, S. M. Kim,

D. Zakharov, E. A. Stach and G. U. Sumanasekera, Preferential growth of single-walled carbon nanotubes with metallic conductivity, *Science*, 2009, **326**, 116–120.

17 P.-X. Hou, W.-S. Li, S.-Y. Zhao, G.-X. Li, C. Shi, C. Liu and H.-M. Cheng, Preparation of Metallic Single-Wall Carbon Nanotubes by Selective Etching, *ACS Nano*, 2014, **8**, 7156–7162.

18 T. Kato and R. Hatakeyama, Growth of Single-Walled Carbon Nanotubes by Plasma CVD, *J. Nanotechnol.*, 2010, **2010**, 1–11.

19 A. R. Muniz, T. Singh and D. Maroudas, Effects of hydrogen chemisorption on the structure and deformation of single-walled carbon nanotubes, *Appl. Phys. Lett.*, 2009, **94**, 103108.

20 G. P. Miller, J. Kintigh, E. Kim, P. F. Weck, S. Berber and D. Tomanek, Hydrogenation of Single-Wall Carbon Nanotubes using Polyamine Reagents: Combined Experimental and Theoretical Study, *J. Am. Chem. Soc.*, 2008, **130**, 2296.

21 W. Lisowski, E. G. Keim, A. H. J. van den Berg and M. A. Smithers, Structural and chemical volution of single-wall carbon nanotubes under atomic and molecular deuterium interaction, *Carbon*, 2005, **43**, 1073.

22 G. Zhang, P. Qi, X. Wang, Y. Lu, D. Mann, X. Li and H. Dai, Hydrogenation and Hydrocarbonation and Etching of Single-Walled Carbon Nanotubes, *J. Am. Chem. Soc.*, 2006, **128**, 6026–6027.

23 F. B. Rao, T. Li and Y. L. Wang, Effect of hydrogen on the growth of single-walled carbon nanotubes by thermal chemical vapor deposition, *Physica E*, 2008, **40**, 779.

24 T. Kato and R. Hatakeyama, Direct growth of short single-walled carbon nanotubes with narrow-chirality distribution by time-programmed plasma chemical vapor deposition, *ACS Nano*, 2010, **4**, 7395–7400.

25 M. J. Behr, E. A. Gaulding, K. A. Mkhoyan and E. S. Aydil, Hydrogen etching and cutting of multiwall carbon nanotubes, *J. Vac. Sci. Technol., B*, 2010, **28**, 1187.

26 S. Niyogi, M. A. Hamon, H. Hu, B. Zhao, P. Bhowmik, R. Sen, M. E. Itkis and R. C. Haddon, Chemistry of Single-Walled carbon Nanotubes, *Acc. Chem. Res.*, 2002, **35**, 1105–1113.

27 Q. Liu, W. Ren, Z.-G. Chen, D.-W. Wang, B. Liu, B. Yu, F. Li, H. Cong and H.-M. Cheng, Diameter-Selective Growth of Single-Walled Carbon Nanotubes with High Quality by Floating Catalyst Method, *ACS Nano*, 2008, **8**, 1722.

28 M. J. Mees, G. Pourtois, E. C. Neyts, B. J. Thijsse and A. Stesmans, Uniform-acceptance force-bias Monte Carlo method with time scale to study solid-state diffusion, *Phys. Rev. B: Condens. Matter*, 2012, **85**, 134301.

29 E. C. Neyts and A. Bogaerts, Combining molecular dynamics with Monte Carlo simulations: implementations and applications, *Theor. Chem. Acc.*, 2013, **132**, 1320.

30 K. M. Bal and E. C. Neyts, On the time scale associated with Monte Carlo simulations, *J. Chem. Phys.*, 2014, **141**, 204104.

31 A. C. T. van Duin, S. Dasgupta, F. Lorant and W. Goddard III, ReaxFF: A Reactive Force Field for Hydrocarbons, *J. Phys. Chem. A*, 2001, **105**, 9396–9409.

32 J. E. Mueller, A. C. T. van Duin and W. A. Goddard III, Development and Validation of ReaxFF Reactive Force Field for Hydrocarbon Chemistry Catalyzed by Nickel, *J. Phys. Chem. C*, 2010, **114**, 4939–4949.

33 E. C. Neyts, Y. Shibuta, A. C. T. van Duin and A. Bogaerts, Catalyzed growth of carbon nanotube with definable chirality by hydrid molecular dynamics – force biased Monte Carlo simulations, *ACS Nano*, 2010, **10**, 6665–6672.

34 U. Khalilov, A. Bogaerts, A. C. T. van Duin and E. C. Neyts, Microscopic mechanisms of vertical graphene and carbon nanotube cap nucleation from hydrocarbon growth precursors, *Nanoscale*, 2014, **6**, 9206–9214.

35 U. Khalilov, A. Bogaerts and E. C. Neyts, Atomic scale simulation of carbon nanotube nucleation from hydrocarbon precursors, *Nat. Commun.*, 2015, **6**, 10306.

36 H. J. C. Berendsen, J. P. M. Postma, W. F. van Gunsteren, A. Di Nola and J. R. Haak, Molecular dynamics with coupling to an external bath, *J. Chem. Phys.*, 1984, **81**, 3684–3690.

37 G. Bussi, D. Donadio and M. Parrinello, Canonical sampling through velocity-rescaling, *J. Chem. Phys.*, 2007, **126**, 014101.

38 T. Ozaki, Variationally optimized atomic orbitals for large-scale electronic structures, *Phys. Rev. B: Condens. Matter Mater. Phys.*, 2003, **67**, 155108.

39 J. P. Perdew, K. Burke and M. Ernzerhof, Generalized gradient approximation made simple, *Phys. Rev. Lett.*, 1996, **77**, 3865–3868.

40 N. Troullier and J. L. Martins, Efficient pseudopotentials for plane-wave calculations, *Phys. Rev. B: Condens. Matter Mater. Phys.*, 1991, **43**, 1993–2006.

41 L. Kleinman and D. M. Bylander, Efficacious form for model pseudopotentials, *Phys. Rev. Lett.*, 1982, **48**, 1425–1428.

42 K. Tada, S. Furuya and K. Watanabe, Ab initio study of hydrogen adsorption to single-walled carbon nanotubes, *Phys. Rev. B: Condens. Matter*, 2001, **63**, 155405.

43 J. S. Arellano, L. M. Molina, A. Rubio, M. J. Lopez and J. A. Alonso, Interaction of molecular and atomic hydrogen with (5,5) and (6,6) single-wall carbon nanotubes, *J. Chem. Phys.*, 2002, **117**, 2281–2288.

44 H. M. Cheng, Q. H. Yang and C. Liu, Hydrogen storage in carbon nanotubes, *Carbon*, 2001, **39**, 1447.

45 W. Andreoni, A. Curioni, J. M. H. Kroes, F. Pietrucci and O. Gronin, Exohedral Hydrogen Chemisorption on a Carbon Nanotube: The Clustering Effect, *J. Phys. Chem. C*, 2012, **116**, 269–275.

46 L. Jeloaica and V. Sidis, DFT investigation of the adsorption of atomic hydrogen on a cluster-model graphite surface, *Chem. Phys. Lett.*, 1999, **300**, 157–162.

47 L. Hornekær, E. Rauls, W. Xu, Ž. Šljivančanin, R. Otero, I. Stensgaard, E. Lægsgaard, B. Hammer and F. Besenbacher, Clustering of Chemisorbed H(D) Atoms on the Graphite (0001) Surface due to Preferential Sticking, *Phys. Rev. Lett.*, 2006, **97**, 186102.

48 A. Nikitin, H. Ogasawara, D. Mann, R. Denecke, Z. Zhang, H. Dai, K. Cho and A. Nilsson, Hydrogenation of Single-

Walled Carbon Nanotubes, *Phys. Rev. Lett.*, 2005, **95**, 225507.
49 A. Nikitin, X. Li, Z. Zhang, H. Ogasawara, H. Dai and A. Nilsson, Hydrogen Storage in Carbon Nanotubes through the Formation of Stable C-H Bonds, *Nano Lett.*, 2008, **8**, 162.
50 G. Buchs, A. V. Krasheninnikov, P. Ruffieux, P. Gröning, A. S. Foster, R. M. Nieminen and O. Gröning, Creation of paired electron states in the gap of semiconducting carbon nanotubes by correlated hydrogen adsorption, *New J. Phys.*, 2007, **9**, 275.
51 N. G. Chopra, L. X. Benedict, V. H. Crespi, M. L. Cohen, S. G. Louie and A. Zettl, Fully collapsed carbon nanotubes, *Nature*, 1995, **377**, 135.
52 X. Sha, B. Jackson and D. Lemoine, Quantum studies of Eley-Rideal reactions between H atoms on a graphite surface, *J. Chem. Phys.*, 2002, **116**, 7158.
53 T. Zecho, A. Güttler, X. Sha, D. Lemoine, B. Jackson and J. Küppers, Abstraction of D chemisorbed on graphite (0001) with gaseous H atoms, *Chem. Phys. Lett.*, 2002, **366**, 188–195.
54 E. C. Neyts, Plasma-Surface Interactions in Plasma Catalysis, *Plasma Chem. Plasma Process.*, 2016, **36**, 185–212.
55 C. Liu, Y. Y. Fan, M. Liu, H. T. Cong, H. M. Cheng and M. S. Dresselhaus, Hydrogen Storage in Single-Walled Carbon Nanotubes at Room Temperature, *Science*, 1999, **286**, 1127.
56 J. M. de Sousa, P. A. S. Autreto and D. S. Galvao, Hydrogenation Dynamics of Twisted Carbon Nanotubes, 2015, ArXiv preprint arXiv: 1510.00265.
57 N. R. Raravikar, P. Keblinski, A. M. Rao, M. S. Dresselhaus, L. S. Schadler and P. M. Ajayan, Temperature dependence of radial breathing mode Raman frequency of single-walled carbon nanotubes, *Phys. Rev. B: Condens. Matter*, 2002, **66**, 235424.
58 T. Halicioglu, Stress calculations for carbon nanotubes, *Thin Solid Films*, 1998, **312**, 11–14.
59 N. Hamada, S. Sawada and A. Oshiyama, New one-dimensional conductors—graphitic microtubules, *Phys. Rev. Lett.*, 1992, **68**, 1579.
60 R. Saito, M. Fujita, G. Dresselhaus and M. S. Dresselhaus, Electronic structure of chiral graphene tubules, *Appl. Phys. Lett.*, 1992, **60**, 2204.
61 E. Joselevich, Electronic Structure and Chemical Reactivity of Carbon Nanotubes: A Chemist's View, *ChemPhysChem*, 2004, **5**, 619–624.
62 G. Henkelman, B. P. Uberuage and H. Jonsson, A Climbing Image Nudged Elastic Band Method for Finding Saddle Points and Minimum Energy Paths, *J. Chem. Phys.*, 2000, **113**, 9901–9904.